Thermal conductivity of amorphous SiO2 by first-principles molecular dynamics

Evelyne Martin, Guido Ori, Thuy-Quynh Duong, Carlo Massobrio, Mauro Boero

Thermal conductivity of amorphous SiO_2 by first-principles molecular dynamics

Evelyne MARTIN[1,*], Guido ORI[2], Thuy-Quynh DUONG[3], Mauro BOERO[2], Carlo MASSOBRIO[2]

1. Université de Strasbourg, CNRS, Laboratoire ICube, UMR 7357, F-67037 Strasbourg, France

2. Université de Strasbourg, CNRS, Institut de Physique et Chimie des Matériaux de Strasbourg, UMR 7504, F-67034 Strasbourg, France

3. Univ. Lille, CNRS, Centrale Lille, Univ. Polytechnique Hauts-de-France, UMR 8520 - IEMN - Institut d'Electronique de Microélectronique et de Nanotechnologie, F-59000 Lille, France.

[*] evelyne.martin@unistra.fr

Abstract

The approach-to-equilibrium molecular dynamics (AEMD) methodology implemented within a first-principles molecular dynamics (FPMD) scheme is applied to amorphous SiO_2. Measurements of the thermal conductivity indicate no reduction down to 10 nm in this technologically relevant material. In view of these premises, we calculate the thermal conductivity of amorphous SiO_2 in the size range comprised between 2 and 8 nm via the AEMD/FPMD approach. The thermal conductivity agrees with experiments for the largest sizes we considered, while it is strongly reduced for values not accessible to experimental resolution (up to 50 % for 2 nm). This behavior is close to that found in glasses chalcogenides $GeTe_4$ and $Ge_2Sb_2Te_5$ within the same AEMD/FPMD approach. Taken together, these results show that the observed decrease of the thermal conductivity is a general feature of disordered networks and in any case cannot be taken as peculiar to a specific class of systems.

I. INTRODUCTION

Amorphous silicon ($aSiO_2$) plays a major role in semiconductor manufacturing i.e. nanoelectronics[1], photovoltaics[2] and renewable energy[3]. While its performances as an electrical insulator can be affected when the thickness is lower than 10 nm as in thin layers (leading to replacement by high-k oxides in transistor grids), several measurements point out that the thermal conductivity is unaffected by size reduction[4]. In particular, data obtained on layers of thickness 8.5 nm up to 3 μm show no changes in this range[5]. Also, Regner *et al.*[6] have measured the dependence of thermal conductivity on the phonon free path in the range 50 nm-1μm via frequency domain thermoreflectance, by showing again no variation. In view of the current dimensions targeted by nanotechnology, the question arises on whether or not thermal conductivity remains constant below 8 nm since if this were the case the behavior of the devices would be dramatically affected.

In what follows, we address this issue by exploiting an atomic scale simulation framework that combines first-principles molecular dynamics (FPMD) within density functional theory (DFT) and the approach-to-equilibrium molecular dynamics (AEMD) technique to extract the thermal conductivity from the transient relaxation of the heat flux. The reasons underlying the use of this methodology are briefly recalled in what follows. In principle, by making use of molecular dynamics, one duly accounts for the compelling anharmonic character of thermal conductivity. However, a compromise has to be found between a reliable treatment of the interatomic forces (requiring a first-principle description) and the computational ressources needed to follow in time the heat flux. To take advantage of the predictive power of FPMD and obtain the thermal conductivity at an accessible cost we employ AEMD in conjunction with FPMD[7–9], as we have done successfully for amorphous $GeTe_4$[10–12] and amorphous $Ge_2Sb_2Te_5$[13]. With this choice, the computational effort is reduced since the transient times inherent in AEMD are much shorter than the time intervals needed to treat the heat flux in alternative MD methods[14,15]. Most importantly, unlike other approaches like the Green-Kubo one[16,17], AEMD is well suited to observe size effects as shown in various kinds of bulk materials and nanostructures[8,9,18,19].

The goal of this paper is to ascertain the presence of size effects for the thermal conductivity of $aSiO_2$ in the range $[2-8]$ nm. This amounts to highlighting nanoscale dimensions for which no experimental results are available. Therefore, our calculations are intended to

confirm or disprove the absence of reduction of thermal conductivity at very small sizes in $aSiO_2$. The paper is organized as follows. In Sec. II we describe the models employed and the preparation of the amorphous system via the use of classical and first-principles molecular dynamics in two successive steps. Details on the MD methodology are also provided. Sec. III presents our calculations on the pair correlation functions and the comparison with analogous results available in the literature, so as to validate our approach. After a brief review of the AEMD basic ideas, Sec. IV reports our results on the thermal conductivity of amorphous SiO_2 as a function of four differents lengths in the direction of the heat flux. These results are critically analyzed in Sec. V. Conclusive remarks are collected in Sec. VI.

II. MODELS AND CALCULATIONS

The prerequisite to the calculation of the thermal conductivity κ is the setup of atomic-scale models for $aSiO_2$. We employed five simulation cells differing by their lengths L in the direction of the heat flux, so as to obtain a trend for $\kappa(L)$ and detect the possible occurrence of size effects. Four values of L have been used (see Table I, where N is the number of atoms in each simulation box). In addition, for one value of L, we considered two distinct cross sections. This allows confirming, as it appeared in several other cases[8,12] that a smaller cross section affects only the statistical uncertainty on the thermal conductivity. Periodic boundary conditions are applied throughout. We stress that, when using AEMD, the periodicity of the system is fully compatible with the existence of a periodic temperature profile that establishes within the system. A brief review of these ideas is given in Sec. IV.

To speed up the production of a system at room temperature, we have resorted to classical molecular dynamics by relying on the good performances of this approach for amorphous SiO_2 when compared to FPMD models. A two step procedure was used, consisting of a first melt-quenching thermal cycle employing the interatomic potential developed by Pedone *et al.*[20] (PMMCS) in its revised and improved version (BMP-harm, Ref. 21) followed by a second thermal cycle using the interatomic potential by Carré *et al.* (CHIK)[22,23]. The initial pairwise interatomic potential PMMCS was chosen because of its reliability and the availability of parameters for many cation-oxygen pairs. Also, its ability to predict the mechanical properties has been well assessed for oxide glasses and oxide nanoparticles. The revised BMP-harm version allows reproducing better the Si-O-Si bond angle distributions

(BADs) and the oxygen distances of the network former. For the second thermal cycle, the CHIK potential was preferred since it stems from a fit to FPMD simulations data, reproducing satisfactorily a set of static and dynamical properties of amorphous SiO_2. Overall, our procedure allowed applying FPMD directly at room temperature on classical MD configurations highly compatible with FPMD ones, thus reducing the computational burden of FPMD-based thermal cycles, especially for the largest system. We stress that our choice is well suited for the case of amorphous SiO_2 since the above classical and first-principles models share the main topological features (predominant tetrahedral coordination, absence of homopolar bonds) unlike in the case of other disordered network-forming systems as chalcogenides. For our classical MD calculations, the leap-frog algorithm encoded in the DL_POLY2.14 package[24] was used to integrate the equations of motion with a time step of 1 fs for both cycles. The initial configurations were generated by randomly positioning the atoms in the simulation box at the experimental density (ρ = 2.2 g cm^{-3}). Quench to lower temperatures was carried out in the framework of the NVT ensemble. As for the first thermal cycle (with the PMMCS potential), the system was heated at T= 5000 K and kept at that temperature for 500 ps, a time ensuring melting and substantial diffusion. Then, the liquids were cooled to 300 K at a cooling rate of 0.6 K/ps, with annealing steps of 500 ps from T= 5000 K down to T= 1000 K every 500 K and every 100 K in the interval 1000 −300 K. The resulting glass structures were subjected to a final equilibration run of 500 ps at 300 K followed by a further thermal cycle via the CHIK potential, bringing back the system to T= 3500 K. At this temperature, atoms have liquid-like diffusion (diffusion coefficients of 7.4×10^{-6} cm^2 s^{-1} for Si and 9.0×10^{-6} cm^2 s^{-1} for O). In this case, the temperature was reduced in the interval 3500 −300 K via a cooling rate of 0.5 K/ps, by adopting the same quenching schedule of the first thermal cycle (namely, same annealing steps and depths of quench in between two temperatures).

Having completed two thermal cycles within classical molecular dynamics, we switched to FPMD for the five cells under consideration by producing a trajectory at room temperature lasting 10 ps, to be made available for the application of AEMD. To this purpose, we resorted to the Car-Parrinello[25] method as implemented in the CPMD code[26]. For the exchange-correlation part of the Kohn-Sham total energy expression, we selected the exchange formula proposed by Becke[27] and the correlation one of Lee, Yang and Parr[28] (BLYP). We described the valence-core interaction by norm-conserving pseudopotentials as prescribed by Troullier

and Martins[29]. Valence electrons are represented by a plane-wave basis set compatible with periodic boundary conditions, with a cutoff of 80 Ry, and expanded at the Γ point only. The mass of the fictitious electronic degrees of freedom was set to 1000 a.u. and the time step to 5 a.u. (0.12 fs) to achieve optimal conservation of the constants of motion. The ionic temperature was controlled with a Nosé-Hoover[30–32] thermostat chain[33]. It should be made clear that, within the above definitions, classical molecular dynamics and first-principles molecular dynamics differ by the nature (classical or quantum) of the calculated forces, both methods being purely classical with respect to the character of the equations of motions, following Newtonian dynamics.

III. MODELS VALIDATION

A crucial step is to ensure the consistency of our models with available FMPD results. To this aim, a reliable benchmark is the calculation of the partial pair correlations functions reported in Fig. 1. The agreement found with the calculations by Giacomazzi *et al.*[34] is excellent, small deviations on the peak positions being due to differences in the selection of the exchange-correlation functions, since the local density approximation (LDA) was employed in Ref. 34. Peak positions and coordination numbers are also in very good agreement with experiments (Table II). This validates our realizations of amorphous SiO_2 as valuable models to study the thermal conductivity in the size range comprised between 2 and 8 nm in the direction of the heat flux.

IV. CALCULATION OF THE THERMAL CONDUCTIVITY

The AEMD methodology creates a periodic thermal profile within the system featuring two blocks kept at different temperatures. This is termed phase 1. Then, the system is left to relax to equilibrium by removing the difference of temperature between the two blocks (phase 2). In practice, during phase 1 two distinct thermostats at temperatures T= 200 K and T= 400 K are applied to the two halves of the computational cell in the direction of the thermal flux (as exemplified in the inset of Fig. 2). Due to the periodic boundary conditions, the signal is periodic as shown by the green curve in Fig. 2 that establishes after a few ps, marking the end of phase 1 (thermostats switched off) and the beginning of phase

2. During phase 2 the temperature profile takes a sinusoidal shape (red curve in Fig. 2) with amplitude decreasing with time. This is exactly a feature of the Fourier equation for the transitory regime of heat transport[7–10].

Another key quantity to be considered is the difference of temperature between the two blocks (averaged over each one of them) converging to zero with an exponential decay (Fig. 3). One can exploit the decay time τ to extract the thermal conductivity κ from the relationship:

$$\kappa = \frac{L^2}{4\pi^2}\frac{C.\rho}{\tau}, \tag{1}$$

where C is the heat capacity calculated from the variation of the total energy versus temperature and τ is determined for each of the five models. A statistical error can be estimated by extending phase 1 via a corresponding phase 2, leading to a second evaluation for τ and κ (Fig. 4).

Results for the thermal conductivity are summarized in 5. As a first observation the results confirm that an increase of the cross section only reduces the error bar. Most notably, we notice that κ increases in the range between 2 and 6 nm reaching eventually an upper limit.

This behavior has been observed in several other systems studied by AEMD[8,9,12,13,18,19] and has been rationalized in Ref. 9. The dependence $\kappa(L)$ is due to non-local effects at short lengths. The $\kappa(L)$ curves obtained by AEMD are well described by the formulation derived by Alvarez and Jou[35] that handles in a single equation both the ballistic and diffusive regime:

$$\kappa_{\mathrm{AJ}}(L) = \kappa_{\mathrm{bulk}}\frac{L^2}{2\pi^2 l^2}\left[\sqrt{1+4\left(\frac{\pi l}{L}\right)^2}-1\right], \tag{2}$$

where κ_{bulk} is the bulk thermal conductivity and l is the mean free path (note that the above equation 2 is employed to draw Fig. 6). On physical grounds, this means that the thermal conductivity has a double regime depending on whether the simulation box is larger or smaller than the mean free path of the heat carriers in the material.

Fig. 5 is indicative of mean free paths taking maximum values around 6 nm in $aSiO_2$. This is the length at which $\kappa(L)$ takes a stationary value, in very good agreement with a set of experimental data available in the literature ($[1.1-1.5]$ W K^{-1} m^{-1}) and reported in Ref. 36. This kind of agreement legitimates our approach and the rationale presented herafter.

V. DISCUSSION

The results given in Fig. 5 provide evidence of a decreasing thermal conductivity for very small sizes, in analogy with what obtained previously for amorphous $GeTe_4$ and amorphous $Ge_2Sb_2Te_5$. These results are collected and compared in Fig. 6.

Thermal conductivities of these materials extend over one order of magnitude, from $GeTe_4$ to $Ge_2Sb_2Te_5$ up to SiO_2. Results obtained for this latter, by far the worst thermal insulator among the three, consolidate previous statements on thermal transport modes in disordered materials reached by using AEMD/FPMD. Fig. 6 shows clearly that Eq. 2 is equally valid for the three materials. Therefore, this allows drawing the general conclusion that the decrease of thermal conductivity with heat propagation length is due to heat carriers taking a mixed ballistic/diffusive character. Upper values of κ as a function of L correspond to mean free paths ranging from 6 nm for SiO_2 to 35 nm for $Ge_2Sb_2Te_5$ and to 50 nm pour $GeTe_4$. This trend is inversely proportional to the value of the thermal conductivity.

Our results do not contradict the absence of any experimental evidence for the reduction of the thermal conductivity at small sizes since no measurements on $aSiO_2$ have been performed in the 2-8 nm range considered here. Similarly there are no such experimental results available for amorphous $GeTe_4$ and $Ge_2Sb_2Te_5$. Concerning other pieces of evidence obtained from calculations, Ref. 37 shows no sensitivity of the thermal conductivty to size reduction (with respect to the bulk value) in a GeTe film with a width of 8 nm[38]. The thermal behavior of this material appears to be closer to the one of amorphous SiO_2 since it would feature, whenever existing, size effects showing up at smaller dimensions than in glasses $GeTe_4$ and $Ge_2Sb_2Te_5$.

In all disordered systems considered so far ($GeTe_4$, $Ge_2Sb_2Te_5$ and SiO_2) size effects manifest themselves on dimensions larger that the structural order inherent in these networks, this order extending on intermediate range scales (10-50 Å at most). This demonstrates that structural disorder can limit heat propagation when compared to crystals (lower values of thermal conductivity and size dependence at smaller dimensions) without totally preventing it. Yet, some of the effects we observed are somewhat unexpected, since the mean free paths of heat propagation turn out to be smaller in a system like amorphous SiO_2, by far more chemically ordered (fewer coordination defects) than $GeTe_4$ and $Ge_2Sb_2Te_5$. Also, our results do not substantiate the assumption that the thermal conductivity of a material

has a strong linear dependence on its intrinsic structural disorder[39]. This calls for further investigations both on the theoretical and experimental side. In particular experiments exploring the range of sizes below 10 nm will be highly instrumental to further improve our understanding of such nanoscale phenomena.

VI. CONCLUSION

We have calculated the thermal conductivity of amorphous SiO_2 by exploiting the approach-to-equilibrium (AEMD) molecular dynamics methodology in conjunction with first-principles molecular dynamics. Our results are based on lengths for heat propagation in between 2 and 8 nm. Beyond 6 nm, thermal conductivity is unchanged, taking an asymptotic value in excellent agreement with experimental results. Below 6 nm, for a range of dimensions unaccessible to experiments, the thermal conductivity of aSiO_2 decreases by a factor of 2 at 2 nm. This reduction confirms analogous trends observed in amorphous $GeTe_4$ and $Ge_2Sb_2Te_5$, by establishing a common pattern among these three systems despite their structural differences (different degrees of chemical order). Overall, our results indicate, in a counterintuitive fashion, that structural disorder can be compatible with the propagation of heat carriers.

VII. ACKNOWLEDGEMENTS

Financial support of the French ANR via the project n. ANR-17-CE09-0039-02 "SIRENA" is gratefully acknowledged. Calculations were performed by using resources from GENCI (Grand Equipement National de Calcul Intensif) (Grants No. 0910296 and 095071). The authors would also like to acknowledge the High-Perfomance Computing (HPC) Center at the University of Strasbourg funded by the Equipex Equip@Meso project (Programme Investissements d'Avenir) and the CPER Alsacalcul/Big Data.

---

[1] H. Zhang, G. Arutchelvan, J. Meersschaut, A. Gaur, T. Conard, H. Bender, D. Lin, I. Asselberghs, M. Heyns, I. Radu, et al., Chemistry of Materials **29**, 6772 (2017).

[2] Y. Xu, W. Chen, X. Ding, X. Pan, L. Hu, S. Yang, J. Zhu, and S. Dai, Inorganic Chemistry Frontiers **5**, 1370 (2018).

[3] A. A. Bhardwaj, J. G. Vos, M. E. S. Beatty, A. F. Baxter, M. T. M. Koper, N. Y. Yip, and D. V. Esposito, ACS Catalysis **11**, 1316 (2021).

[4] M. C. Wingert, J. Zheng, S. Kwon, and R. Chen, Semiconductor Science and Technology **31**, 113003 (2016).

[5] A. J. Griffin, F. R. Brotzen, and P. J. Loos, Journal of Applied Physics **75**, 3761 (1994).

[6] K. T. Regner, D. P. Sellan, Z. Su, C. H. Amon, A. J. McGaughey, and J. A. Malen, Nature Communications **4**, 1640 (2013).

[7] E. Lampin, P. L. Palla, P.-A. Francioso, and F. Cleri, Journal of Applied Physics **114**, 033525 (2013).

[8] H. Zaoui, P. L. Palla, F. Cleri, and E. Lampin, Physical Review B **94**, 054304 (2016).

[9] P. L. Palla, S. Zampa, E. Martin, and F. Cleri, International Journal of Heat and Mass Transfer **131**, 932 (2019).

[10] A. Bouzid, H. Zaoui, P. L. Palla, G. Ori, M. Boero, C. Massobrio, F. Cleri, and E. Lampin, Physical Chemistry Chemical Physics **19**, 9729 (2017).

[11] E. Martin, P. L. Palla, F. Cleri, A. Bouzid, G. Ori, S. Le Roux, M. Boero, and C. Massobrio, Journal of Non-Crystalline Solids **498**, 190 (2018).

[12] T.-Q. Duong, C. Massobrio, G. Ori, M. Boero, and E. Martin, Physical Review Materials **3**, 105401 (2019).

[13] T.-Q. Duong, A. Bouzid, C. Massobrio, G. Ori, M. Boero, and E. Martin, RSC Advances **11**, 10747 (2021).

[14] D. P. Sellan, E. S. Landry, J. E. Turney, A. J. H. McGaughey, and C. H. Amon, Physical Review B **81**, 214305 (2010).

[15] H. Dong, Z. Fan, L. Shi, A. Harju, and T. Ala-Nissila, Physical Review B **97**, 094305 (2018).

[16] Y. He, I. Savić, D. Donadio, and G. Galli, Physical Chemistry Chemical Physics **14**, 16209 (2012).

[17] J. M. Larkin and A. J. H. McGaughey, Physical Review B **89**, 144303 (2014).

[18] H. Zaoui, P. L. Palla, F. Cleri, and E. Lampin, Physical Review B **95**, 104309 (2017).

[19] H. Zaoui, P. L. Palla, S. Giordano, F. Cleri, M. Verdier, D. Lacroix, J.-F. Robillard, K. Termentzidis, and E. Martin, International Journal of Heat and Mass Transfer **126**, 830 (2018).

[20] A. Pedone, G. Malavasi, M. C. Menziani, A. N. Cormack, and U. Segre, The Journal of Physical Chemistry B **110**, 11780 (2006).

[21] M. Bertani, M. C. Menziani, and A. Pedone, Physical Review Materials **5**, 045602 (2021).

[22] A. Carré, J. Horbach, S. Ispas, and W. Kob, EPL (Europhysics Letters) **82**, 17001 (2008).

[23] A. Carré, S. Ispas, J. Horbach, and W. Kob, Computational Materials Science **124**, 323 (2016).

[24] W. Smith and T. Forester, Journal of Molecular Graphics **14**, 136 (1996).

[25] R. Car and M. Parrinello, Physical Review Letters **55**, 2471 (1985).

[26] Jointly by IBM Corporation and by Max Planck Institute, Stuttgart, *CPMD code* (2020), URL `http://www.cpmd.org`.

[27] A. D. Becke, Physical Review A **38**, 3098 (1988).

[28] C. Lee, W. Yang, and R. G. Parr, Physical Review B **37**, 785 (1988).

[29] N. Troullier and J. L. Martins, Physical Review B **43**, 1993 (1991).

[30] S. Nosé, Molecular Physics **52**, 255 (1984).

[31] S. Nosé, The Journal of Chemical Physics **81**, 511 (1984).

[32] W. G. Hoover, Physical Review A **31**, 1695 (1985).

[33] G. J. Martyna, M. L. Klein, and M. Tuckerman, The Journal of Chemical Physics **97**, 2635 (1992).

[34] L. Giacomazzi, P. Umari, and A. Pasquarello, Physical Review B **79**, 064202 (2009).

[35] F. X. Alvarez and D. Jou, Applied Physics Letters **90**, 083109 (2007).

[36] R. Anufriev, S. Tachikawa, S. Gluchko, Y. Nakayama, T. Kawamura, L. Jalabert, and M. Nomura, Applied Physics Letters **117**, 093103 (2020).

[37] D. Campi, D. Donadio, G. C. Sosso, J. Behler, and M. Bernasconi, Journal of Applied Physics **117**, 015304 (2015).

[38] G. C. Sosso, D. Donadio, S. Caravati, J. Behler, and M. Bernasconi, Physical Review B **86**, 104301 (2012).

[39] L. Qiu, N. Zhu, Y. Feng, E. E. Michaelides, G. Żyła, D. Jing, X. Zhang, P. M. Norris, C. N. Markides, and O. Mahian, Physics Reports **843**, 1 (2020).

[40] Q. Mei, C. J. Benmore, S. Sen, R. Sharma, and J. L. Yarger, Physical Review B **78**, 144204 (2008).

Figures

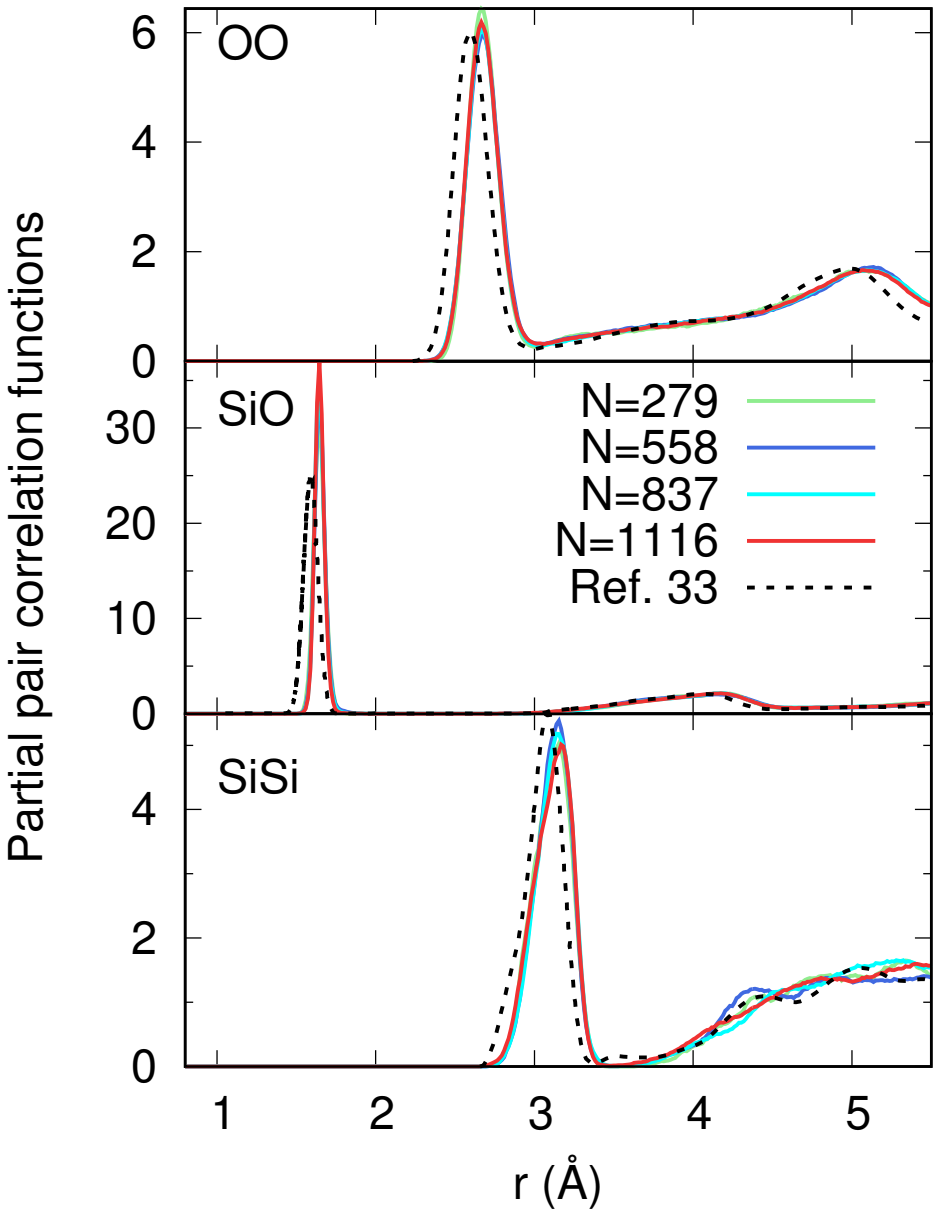

FIG. 1: Partial pair correlation functions of the models of amorphous SiO_2, compared to the result by Giacomazzi *et al.* (Ref. 34). For $N = 558$ atoms, the result shown is for the model with the rectangular cross section.

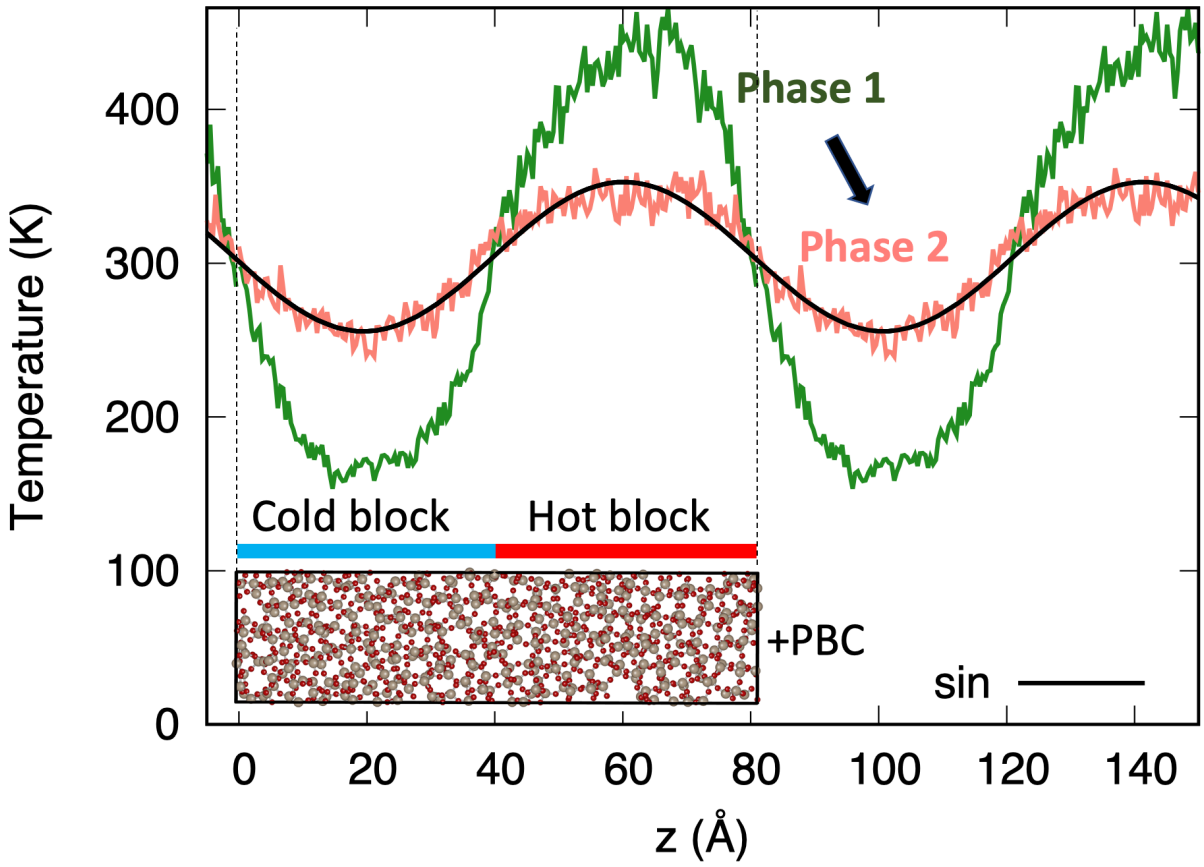

FIG. 2: Temperature profile in the main simulation box and in its replicas for the N= 1116 case. Green line: the profile is averaged over the whole phase 1. Red line: the profile is averaged over the whole phase 2. Note that the profile is sinusoidal during phase 2 (black line, fit to the data).

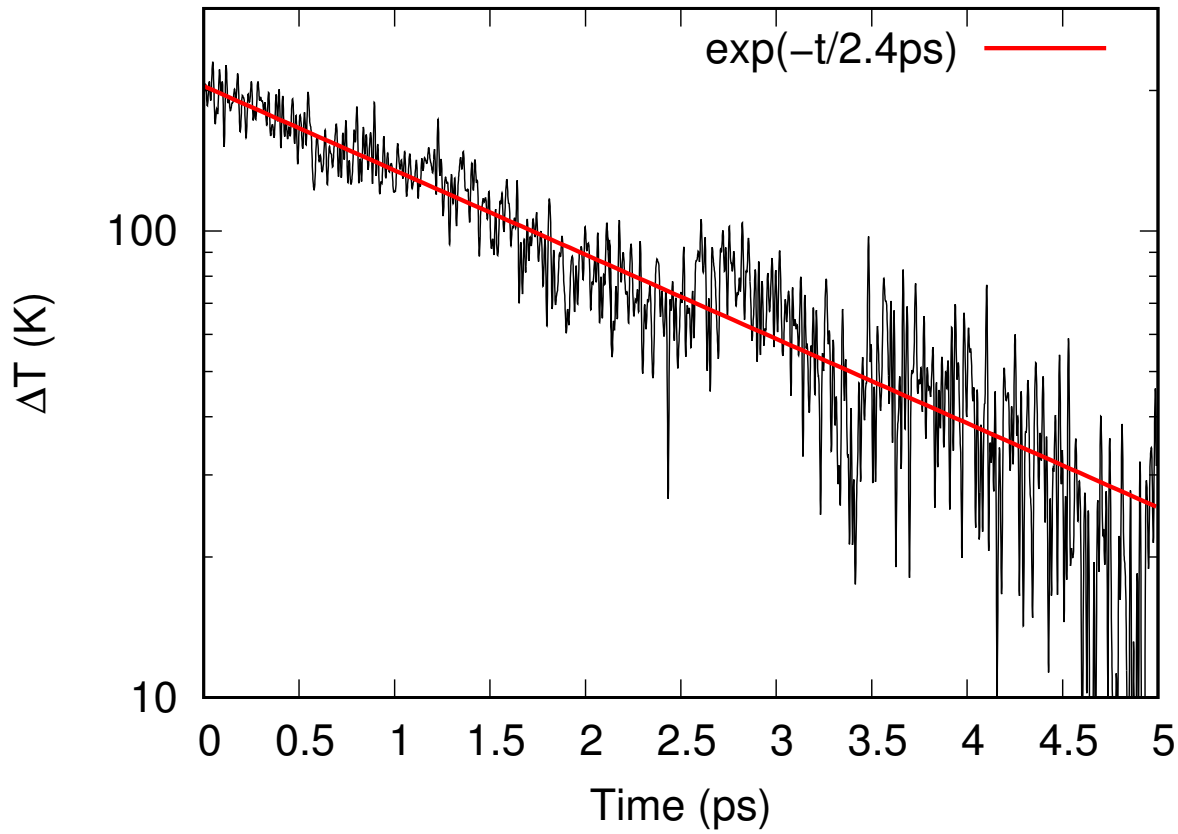

FIG. 3: Evolution of the temperature difference between hot and cold blocks during phase 2 of AEMD (black line) together with a fit to an exponential decay (red line). We are considering here the case of $N = 837$, second trajectory (extended phase 1, see text).

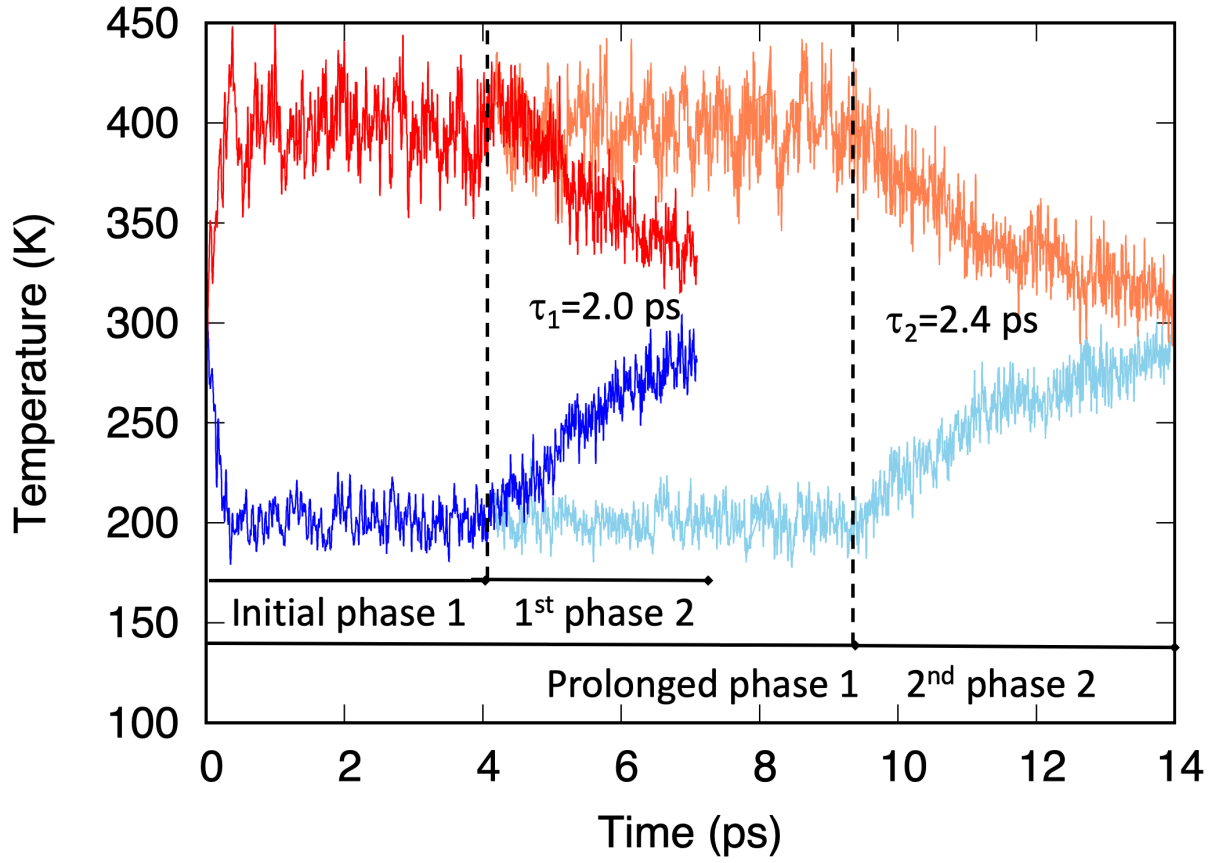

FIG. 4: Temperature evolution in the hot (red lines) and cold (blue lines) blocks during phase 1 and phase 2 of AEMD. Two calculations are performed to allow estimating the statistical error. A phase 1 lasting 4 ps (named "Initial phase 1") is followed by a phase 2 (shown by bold red (hot) and bold blue (cold) colors). A second phase 1 (extension of the first by 5 ps, named "Prolonged phase") is followed by a second phase 2 (shown by light red (hot) and light blue (cold) colors). We obtain two decay times τ equal to 2.0 et 2.4 ps for the case N=837.

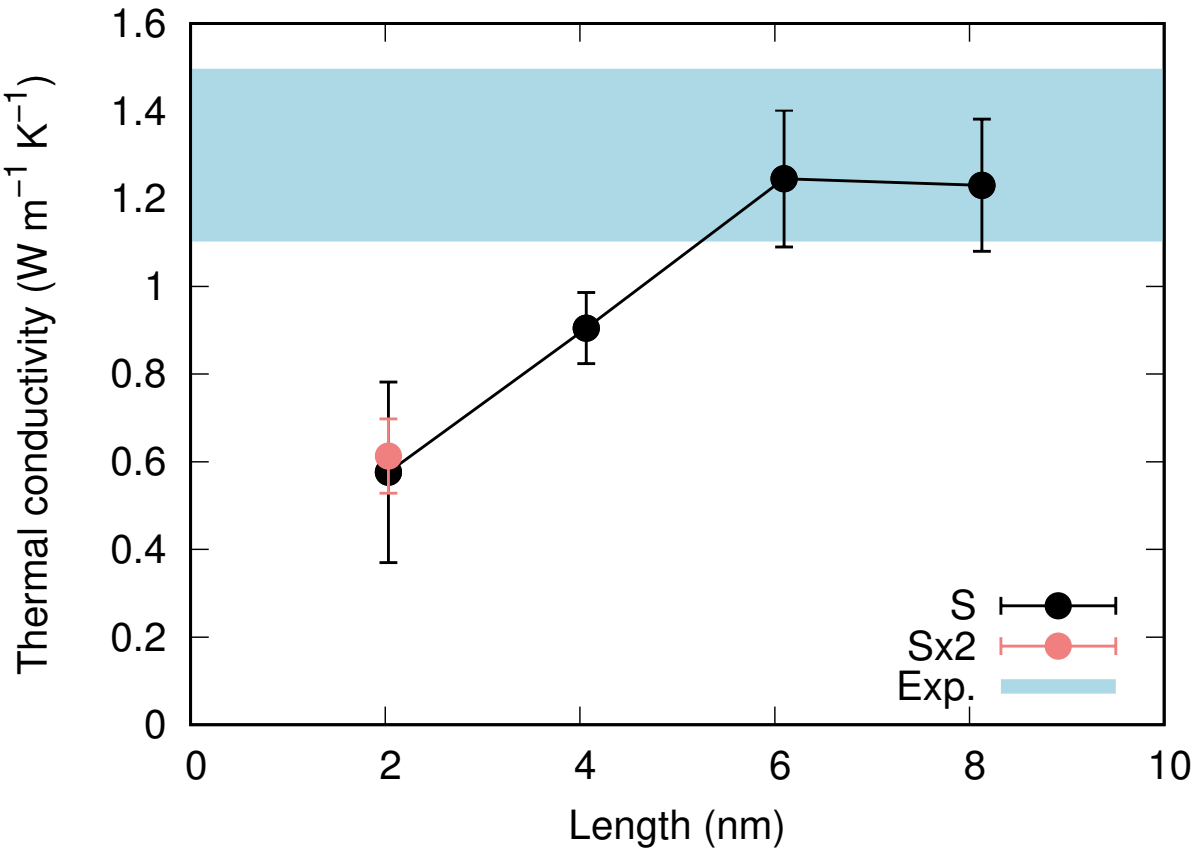

FIG. 5: Thermal conductivity of amorphous SiO_2 as a function of length in the direction of the heat flux in between 2 et 8 nm (black dots for section S=10.16×20.32 Å^2 and coral dots for section $S \times 2$=20.32×20.32 Å^2). The error bars have been obtained by taking advantage of distinct calculations for each size (see Fig. 4). The shaded blue area has been drawn to include different experimental values obtained with various techniques.

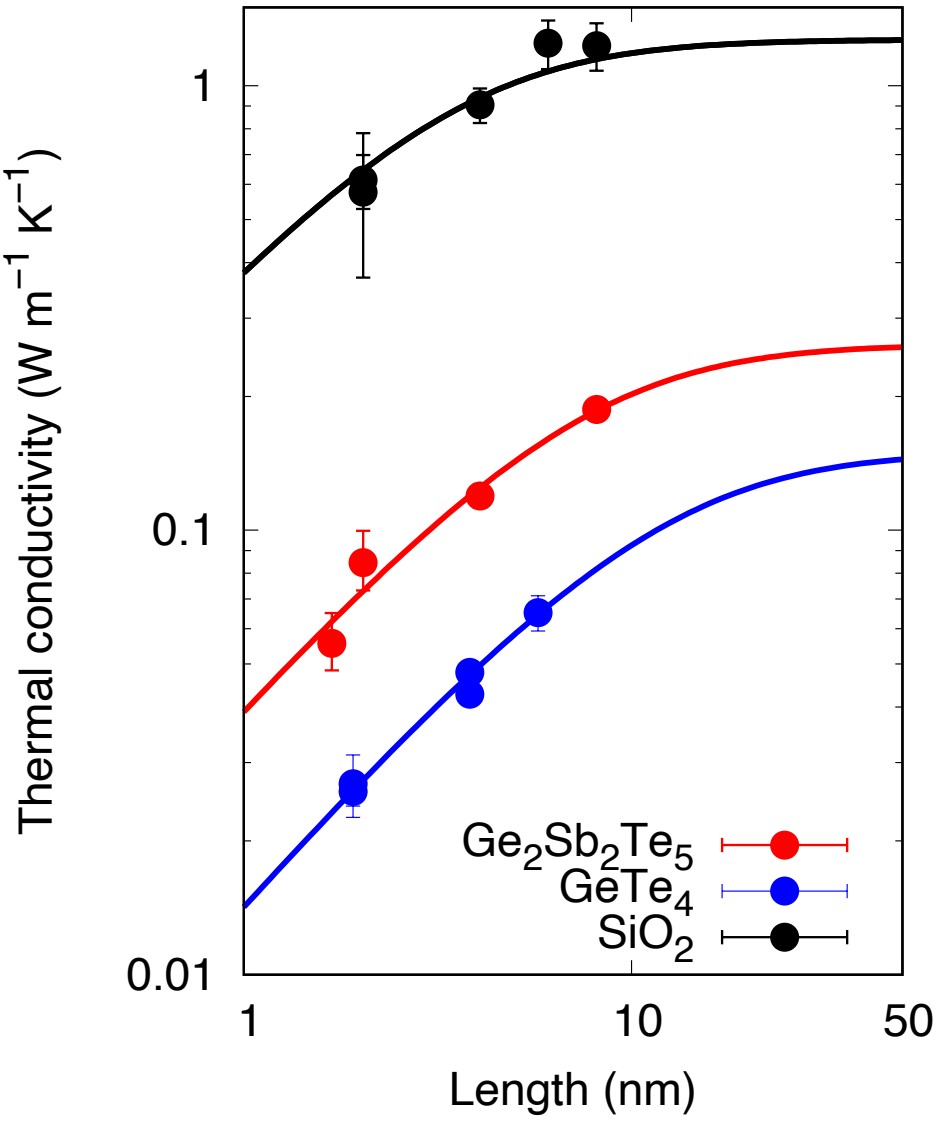

FIG. 6: Thermal conductivity of amorphous SiO_2 (black dots), $GeTe_4$[10–12] (blue dots) and $Ge_2Sb_2Te_5$[13] (red dots)) as a function of L. We have superposed Eq. 2 (lines with corresponding colors) to the results of our calculations (dots).

Tables

TABLE I: Models of amorphous SiO_2 employed in this work. L is the supercell length in the heat transport direction. S is the cross section.

N	279	558	558	837	1116
L (Å)	20.32	20.32	40.64	60.96	81.28
S (Å^2)	10.16×20.32	20.32×20.32	10.16×20.32	10.16×20.32	10.16×20.32

TABLE II: Peak positions and coordination numbers (obtained by integrating up to the first minima of the pair correlation functions) compared to experiments from Ref. 40.

	Si-Si		Si-O		O-O	
	This work	Expt.	This work	Expt.	This work	Expt.
Peak position (Å)	3.17	3.08	1.64	1.60	2.66	2.62
Coordination number	4	4.06	4	3.89	6.3	5.99